Dawn of a new era in industrial photochemistry: Scale up of micro- and meso-structured photoreactors

Emine Kayahan‡[1], Mathias Jacobs‡[1], Leen Braeken[1,2], Leen C.J. Thomassen[1,2], Simon Kuhn[2], Tom van Gerven[2], M. Enis Leblebici*[1,2]

[1]Center for industrial process technology, Department of Chemical Engineering, KU Leuven, Diepenbeek, Belgium

[2]Process Engineering for Sustainable Systems, Department of Chemical Engineering, KU Leuven, Leuven, Belgium

Email: M. Enis Leblebici - muminenis.leblebici@kuleuven.be

* Corresponding author

‡ Equal contributors

Abstract

Photochemical activation routes are gaining the attention of the scientific community since they can offer an alternative to the traditional chemical industry that mainly utilizes thermochemical activation of molecules. Photoreactions are fast and selective which would potentially reduce the downstream costs significantly if the process is optimized properly. With the transition towards green chemistry, the traditional batch photoreactor operations are becoming abundant in this field. Process intensification efforts led to micro- and meso-structured flow photoreactors. In this work, we are

reviewing structured photoreactors by elaborating on the bottleneck of this field: development of an efficient scale up strategy. In line with this, micro- and meso-structured bench scale photoreactors were evaluated based on a new benchmark called photochemical space time yield ($mol \cdot day^{-1} \cdot kW^{-1}$) which takes into account the energy efficiency of the photoreactors. It was manifested that along with the selection of photoreactor dimensions and appropriate light source, optimization of process conditions such as residence time and concentration of the photoactive molecule is also crucial for an efficient photoreactor operation. In this paper, we are aiming to give a comprehensive understanding for scaling up strategies by benchmarking selected photoreactors and by discussing transport phenomena in several other photoreactors.

Keywords

Microreactor scale-up; microreactor; monolith reactors; packed bed reactor; photoreactor scale-up

Introduction

In traditional chemical industry, thermochemical activation routes are mostly preferred. Light can also activate some molecules which lead to fast and selective reaction pathways. Photochemistry spans a number of reactions. For organic chemistry, 8000 photoreactions has been listed since 1975 [1]. Despite the huge portfolio, there is a lack of industrial applications of photochemistry. Van Gerven et al. listed five industrial application of photochemistry in commercial wastewater treatment installations [2]. In addition, Artemisinin, which is a drug to treat malaria, was produced in an industrial scale photoreactor in a Sanofi production facility in Italy [3]. Furthermore, the production of some fine chemicals such as ε-caprolactam, rose oxide and vitamin D

on an industrial scale is already proven to be successful [4]. These examples show that photochemistry is a viable alternative for conventional chemistries. In addition to specialty chemicals and wastewater treatment, photochemical pathways can also be used for methanol production [5], N_2 fixation [6] and CO_2 sequestration [7]. Still, photochemistry has not been exploited much in industry since distribution of light inside a photoreactor brings a lot of complexity to the reactor design. Unlike thermochemical reactions, it is not feasible to scale-up photoreactions by increasing the dimensions of the reactor due to the exponential attenuation of light. Non-uniform light distribution often leads to a lower selectivity and longer reaction times which, in turn, lowers the productivity [8], [9]. Since photoreactions are intrinsically quite fast, mass transfer limitations should also be taken into account while designing multiphase photoreactors, this complicates the design even further [10].

Photoreactions are typically performed in batch reactors. With the process intensification efforts towards green chemistries, continuous flow technologies, micro- and meso-structured flow photoreactors have emerged as alternatives to batch operation. Due to the small characteristic length of microreactors, more uniform light distribution could be obtained. Elimination of over-irradiation or dark zones results in less side product formation. Mass transfer limitations can be alleviated in these photoreactors with the help of various catalyst structures, beads, static mixers and/or Taylor flow [4], [11]. In addition, these reactors allow safer operation since it is easier to control the overheating and handling hazardous chemicals in smaller volumes [4], [11]. In addition to photomicroreactors, micro- and meso-structures in larger scale photoreactors such as packed beds and monoliths coated with catalysts can also enhance the mass transfer and operate at microreactor reaction rates. Together with

photomicroreactors, these structured reactors are opening a new era in photochemistry by providing a platform for enhancing the photoreaction rates and easier scale-up.

One of the hurdles in scaling up of photoreactors is the lack of consensus on a benchmark to compare different scales and geometries. The simplest benchmark is the apparent rate constant *k* [12]–[15] shown in Equation 1.

$$k_{app}[s^{-1}] = \frac{c_0[mol \cdot m^{-3}] - c\,[mol \cdot m^{-3}]}{c\,[mol \cdot m^{-3}] \cdot \tau\,[s]} \quad (1)$$

where c_0 is the initial concentration, *c* the concentration at the end of the reaction and τ is the residence time.

The comparison of the reaction rate constants for different reactor types such as a photomicroreactor and a batch photoreactor are often used to point out how much the reactor design could change the performance of photoreactions. Takei et al. reported a reaction rate that is 70 times higher in a photomicroreactor compared to a batch cuvette with the same yield for the synthesis of L-pipecolinic acid [16]. The rate of methylene blue reduction was increased more than 150 times in a photomicroreactor compared to a batch system [17]. Still, it should be kept in mind that such comparisons are often strongly biased due to the difference in photons absorbed in different reactor geometries and the possible difference in mass transfer limitations. Another benchmark is the quantum yield Φ. This is defined by the IUPAC as the number of defined events occurring per photon absorbed by the system. This is shown in Equation 2.

$$\Phi\left[\frac{mol}{einstein}\right] = \frac{amount\ of\ reactant\ consumed\ or\ product\ formed\ [mol]}{\text{amount of photons absorbed } [einstein]} \quad (2)$$

The photonic efficiency ξ (Equation 3) is defined by the IUPAC as the ratio of the reaction rate to the rate of incident photons within a defined wavelength interval [18]. This benchmark expresses light efficiency. However, it does not provide information about the productivity.

$$\xi[-] = \frac{r\ [mol \cdot s^{-1}]}{\varphi\ [einstein \cdot s^{-1}]} \quad (3)$$

where *r* is the reaction rate φ is the rate of incident photons.

The aforementioned benchmarks focus on the efficiency of the photochemical process and do not consider the photon transport to the reactor, energy utilization and throughput, thus are not suitable for comparing the scaled-up photoreactors. Space-time yield (STY), which is the amount of product produced per unit of time and reactor volume is often used to compare scaled up (non-photo) reactors, which is shown in Equation 4 [19]. However, this benchmark does not include the energy consumption of the lamp utilized to provide the necessary energy. In a study of Leblebici et al., a new benchmark, photochemical space-time yield (PSTY), was proposed and used to compare different photoreactors as shown in Equation 5. This benchmark relates the productivity and energy efficiency. Therefore, it is commonly applied in recent studies to assess the scalability of the process [15], [20]–[22].

$$STY\left[\frac{mol}{m^3 \cdot s}\right] = \frac{n\ [mol]}{V_{reactor}\ [m^3] \cdot t\ [s]} = \frac{C_0[mol \cdot m^{-3}] \cdot X_a[-]}{\tau\ [s]} \quad (4)$$

$$PSTY\ \left[\frac{mol}{kW \cdot\ day}\right] = \frac{STY\ [mol \cdot m^{-3} \cdot s^{-1}]}{P\ [kW]/V_{reactor}(m^3)} \quad (5)$$

where STY is the space time yield, n is the amount of product produced, t is the time, $V_{reactor}$ is the reactor volume, C_0 is the starting concentration, X_a is the conversion, τ is the residence time, PSTY is the photocatalytic space time yield and P is the lamp power.

In this paper, together with the photomicroreactors, larger scale photoreactors which contains micro- and meso-structures, since their performance and the problems related to scaling up are comparable. Our aim is to give an overview of the scale up of photochemical reactions by discussing transport phenomena and technical challenges. In addition, we are assessing several high-throughput structured photoreactors using PSTY to reveal the successful scale up strategies in literature.

Design considerations

The complexity of the photochemical processes leads to significant challenges in the photoreactor design. In addition to the general reactor design consideration such as selection of a suitable reactor material and geometry, selection of a proper light source needs to be considered. The reactor material should be inert to the reaction medium and transparent to the wavelength range that drives the photochemical reaction. Ideally, the light source should emit light only in the wavelength range of interest and should have high energy efficiency. In addition, the solvent should not absorb light strongly nor be a quencher of the photoreaction. In order to avoid excessive heating of the light source, cooling systems might be necessary. The distribution of light inside the reactor brings a lot of complexity into the design. Since most photoactive molecules are strong absorbers of light, light usually decays in a few millimeters in a photoreactor. That limits dimensions of the photoreactors. As a result, many

photoreactor units are usually required to achieve the desired throughput. In order to obtain similar reaction conditions, flow needs to be distributed to all photoreactor units uniformly. In heterogeneous reactions, the flow field also affects mass transport significantly. Structures such as beads or monoliths are frequently used to enhance mass transfer, which, in turn, affect the flow field. If the photoactive molecule is the reactant, it depletes as the reaction proceeds. That introduces more variation in the light field depending on the degree of mixing and reaction rate. Due to the interplay of different transport phenomena, a mathematical description is often needed for a proper reactor design. Flow field (momentum transport), mass transport and light field (radiative transport) needs to be coupled to compute reaction kinetics (Figure 1) [11].

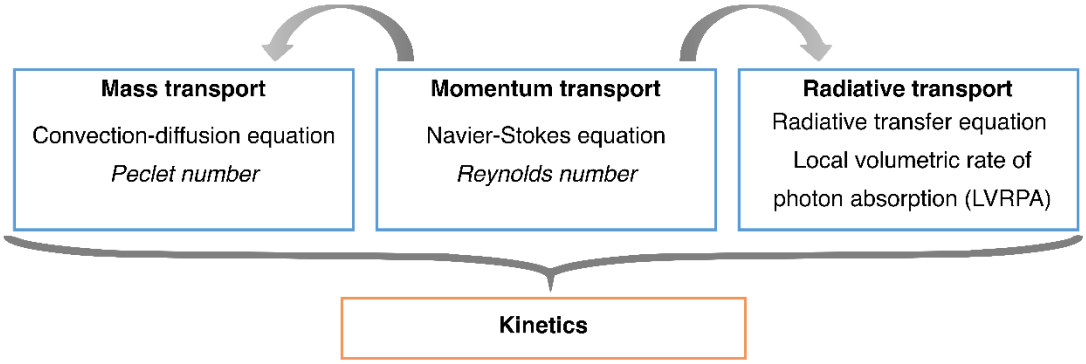

Figure 1. The momentum transport affects the mass transfer and the light field. All transport phenomena needs to be coupled to compute the kinetics.

Microstructured chips used in photochemistry have various channel geometries such as straight line, serpentine, square serpentine, spiral as shown in Figure 2. Serpentine and square serpentine are used to increase the residence time and for mixing. Microcapillaries (Figure 2f) wrapped around a light cylinder are also commonly used in photochemistry.

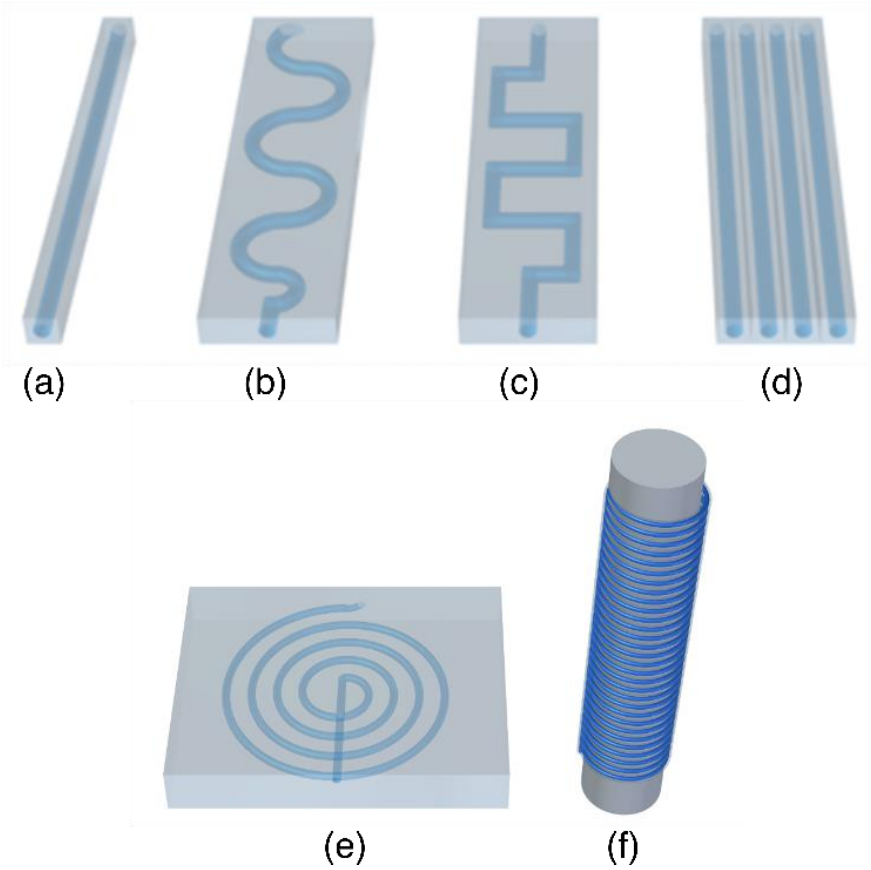

Figure 2. Common photomicroreactor designs (a) Straight channel (b) Serpentine channel (c) Square serpentine channel (d) planar microchannel array (e) Spiral-shaped microreactor (f) Capillary photomicroreactors.

While designing microreactors, it is important to distinguish different applications. The lab-on-a-chip concept has enabled researchers to work on intrinsic kinetics. Intrinsic data acquisition is crucial while designing and operating large-scale reactors. Several microreactors such as spiral channel microreactor carved on a flat aluminum plate [23], a capillary tube [24], a microchannel cast and cured on polydimethylsiloxane (PDMS) slab [25] or a rectangular slab micromachined on a Teflon [26] were used for determining intrinsic kinetics of different photochemical reactions. Such demonstrations suggest that if they are scaled up properly, microreactors could be operated with intrinsic kinetics. That would reduce reactor size and downstream processing costs while increasing safety. The design considerations of the

microreactors which aim at large-scale chemical synthesis are significantly different than lab on chip concept. While gathering intrinsic kinetic data, energy efficiency is not a concern. Optimal photon flux should be provided to make sure that the reactor is operated without light transfer limitations. In addition, utilization of one microchannel or a capillary tube would be enough as long as there is adequate mixing to overcome mass transfer limitations in multiphase reaction systems. On the other hand, studies aiming at scale up of microreactors should consider the distribution of flow and light to all units of microreactors as well as the energy efficiency. A systematic scale up strategy would be to increase the concentration of the chemicals and the reactor dimensions by keeping the yield constant while assessing the energy efficiency of the photoreactor by using benchmarks such as PSTY. Then, the best reactor dimensions and operational parameters could be chosen. The PSTY of several photoreactor designs were discussed in the next section.

Scaling up and energy efficiency

Photoreactors cannot be scaled up by the conventional dimension enlarging strategy due to the light attenuation effect. Heterogeneous flow dynamics and light field complicate the design further. As a result, photochemical processes are hard to predict and scale up. Several large-scale slurry reactor designs for multiphase reactions such as the fountain reactor [27], fluidized bed reactor [28] and spinning disc reactors [29], [30] have been utilized in the field of photochemistry. Although such large-scale slurry reactors can improve the mass transfer, distributing light properly in a large-scale slurry reactor remains a challenge. Rapid attenuation of light inside photoreactors limits the dimensions of photoreactors. As a result, microstructured reactors are gaining more attention from researchers in this field. Leblebici et al. compared twelve

commonly used photoreactor designs [22]. The microstructured reactor [25] resulted in the highest STY but the lowest PSTY due to high power consumption of the light source [22]. In that work, a 120 W UV light source was used to illuminate 1.5 µL of reactor [25]. However, with the selection of a proper light source along with a systematic scale up strategy by increasing reactor dimensions and concentration of the absorbing species gradually, microstructured photoreactors have the potential to score the highest PSTYs. It is also important to note that PSTY does not account for the quantum yield. Therefore, the molecular and electronic features of the reactants which could significantly affect PSTY values are not accounted for when comparing different reactions. Therefore, it is hard to make global conclusions just by looking at PSTY values especially when intermolecular and intramolecular reactions or homogenous and heterogenous reactions are compared. Since quantum yields of most photochemical reactions are not known, PSTY still gives a nice comparison between different reactor geometries. PSTY especially gains importance while characterizing and deciding on the operational conditions of a photoreactor when a specific photoreaction needs to be scaled up.

Flow and light need to be distributed properly to all units of the microstructured reactors while scaling up in order to ensure the same reaction conditions everywhere. For multiphase reactions, mass transfer issues need to be tackled with the design, as well. Microreactors could be scaled up by numbering up channels, which is also referred to as scaling out, or scaled up by enlarging dimensions of microchannels. Another way of scaling up of reactors which can work with intrinsic kinetics is to create micro- or meso-structures in large vessels. Translucent packed bed reactors and aerosols

photoreactor are examples of such designs. Below, we are discussing several scale-up strategies applied in photochemistry.

Most researchers that utilize photomicroreactors suggest that scaling up could be achieved by numbering up. One of the most used photomicroreactors are capillaries wrapped around a light source. Such microcapillaries could be scaled up by connecting them either in parallel or in series (Figure 3a and b). In a previous study, five polymer-based microcapillaries with a length of 11.5 m and an inner diameter of 0.8 mm were wrapped around two Pyrex glass columns. UV-lamps were placed inside the glass columns. A representative set-up is given in Figure 3a. The addition of isopropanol to 2(5H)-furanone in the presence of the photosensitizer, 4,4'-dimethoxy-benzophenone (DMBP), was studied. A single multi-syringe pump was used to supply the reactants to the photomicroreactors. This kind of scaling up is called external numbering up since each reactor is fed directly by the pump. This numbering up strategy allowed running ten parallel microreactors at the same time. This microreactor set-up used 30% less energy than the batch reactor without the requirement for cooling [31]. The PSTY of this paper was calculated when the same reaction was performed at the same time in ten parallel reactors (Table 1**Error! Reference source not found.**- entry 1). The reactions that are presented in Table 1**Error! Reference source not found.** are shown in Figure 4**Error! Reference source not found.**. The PSTY was around 9.5 $mol \cdot day^{-1} \cdot kW^{-1}$ when the yield was 72%. To achieve almost complete conversion (94%), the residence time was increased twice. That decreased the PSTY to 6.26 $mol \cdot day^{-1} \cdot kW^{-1}$. Still, this microcapillary reactor outperformed all the rest of the reactors that were compared in this paper. That is because large reactor volume (10 x 5 mL) was illuminated effectively with two low power lamps (2 x 18 W).

In addition, several photosensitizer and reactant concentrations were screened before the reaction was scaled up. With the selected photosensitizer concentration (10 mM), the light transmission through the 0.8 mm diameter microcapillary was around 65%. Higher DMBP concentration caused precipitations and resulted in a lower yield. Lower DMBP concentrations decreased the yield significantly, which decreases PSTY values around 6-folds (data not shown). In another work, the same group reported the use of the same reaction in a commercial microchip (Micronit Microfluidics FC_R150.676.2) with an internal volume of 15 µm. This microchip was illuminated with 6x75 mW LEDs. The DMBP concentration was 6.7 mM which results in around 95% light transmission through 150 µm channel depth of the microreactor [32]. This reactor had a PSTY of 0.57 $mol \cdot day^{-1} \cdot kW^{-1}$ (Table 1**Error! Reference source not found.**, entry 3). Although the same reaction and similar conversions were achieved in these two photomicroreactors [31], [32], the PSTY was more than ten times lower in the microchip. This is potentially due to the difference in the volumes and the fraction of photons absorbed in two different photomicroreactors. These results illustrate that choosing a proper light source and adjusting the concentrations would improve the PSTY significantly, leading to an efficient scale up of photomicroreactors.

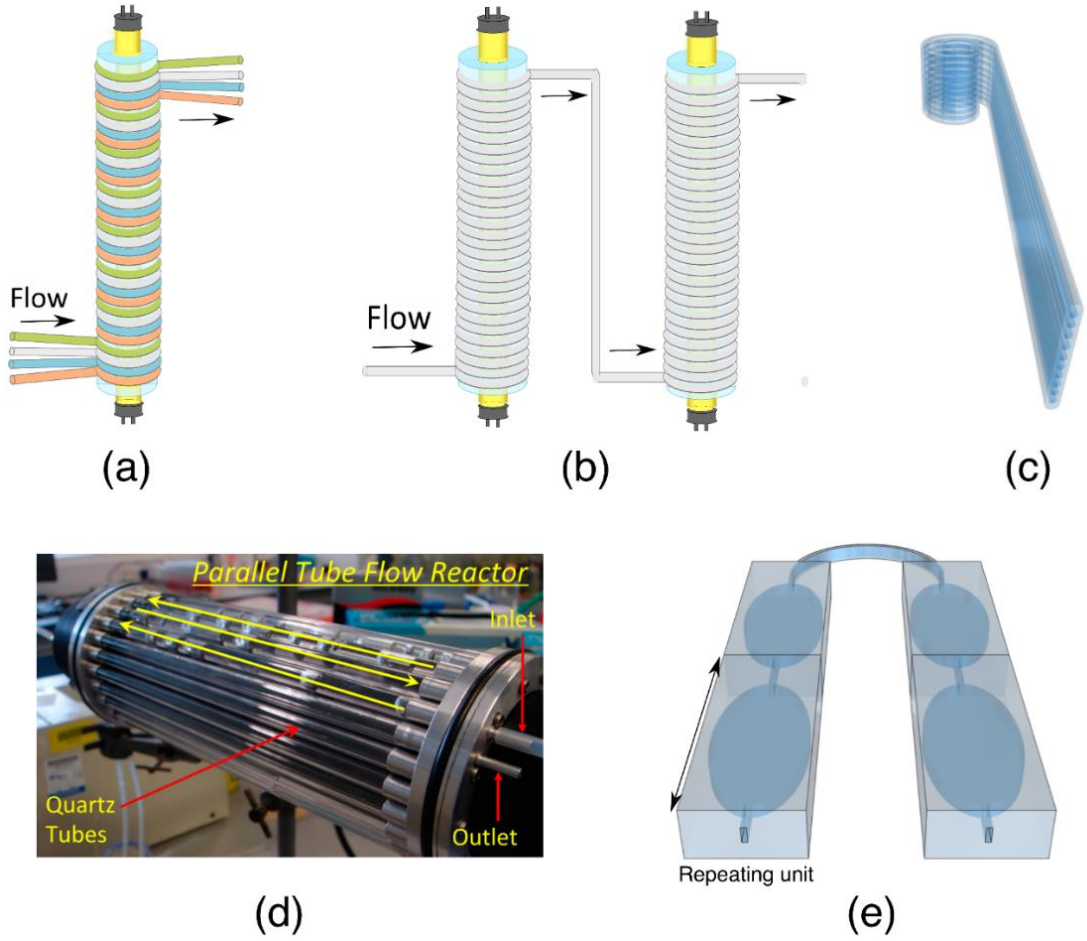

Figure 3. Benchmarked photoreactors (a) Microcapillaries in parallel (b) Microcapillaries in series (c) Fluoropolymer microcapillary films (d) Firefly reactor. Reprinted from *A small-footprint, high-capacity flow reactor for UV photochemical synthesis on the kilogram scale* L. D. Elliott, M. Berry, B. Harji, D. Klauber, J. Leonard, and K. I. Booker-Milburn, Org. Process Res. Dev., vol. 20, pp. 1806–1811, 2016, [33], DOI: 10.1021/acs.oprd.6b00277, licensed under a Creative Commons Attribution 4.0 International license, https://creativecommons.org/licenses/by/4.0/. (e) internal + external numbering-up of a microreactor unit. The image is reproduced by the authors' of this article to illustrate the microreactor structures reported in [34].

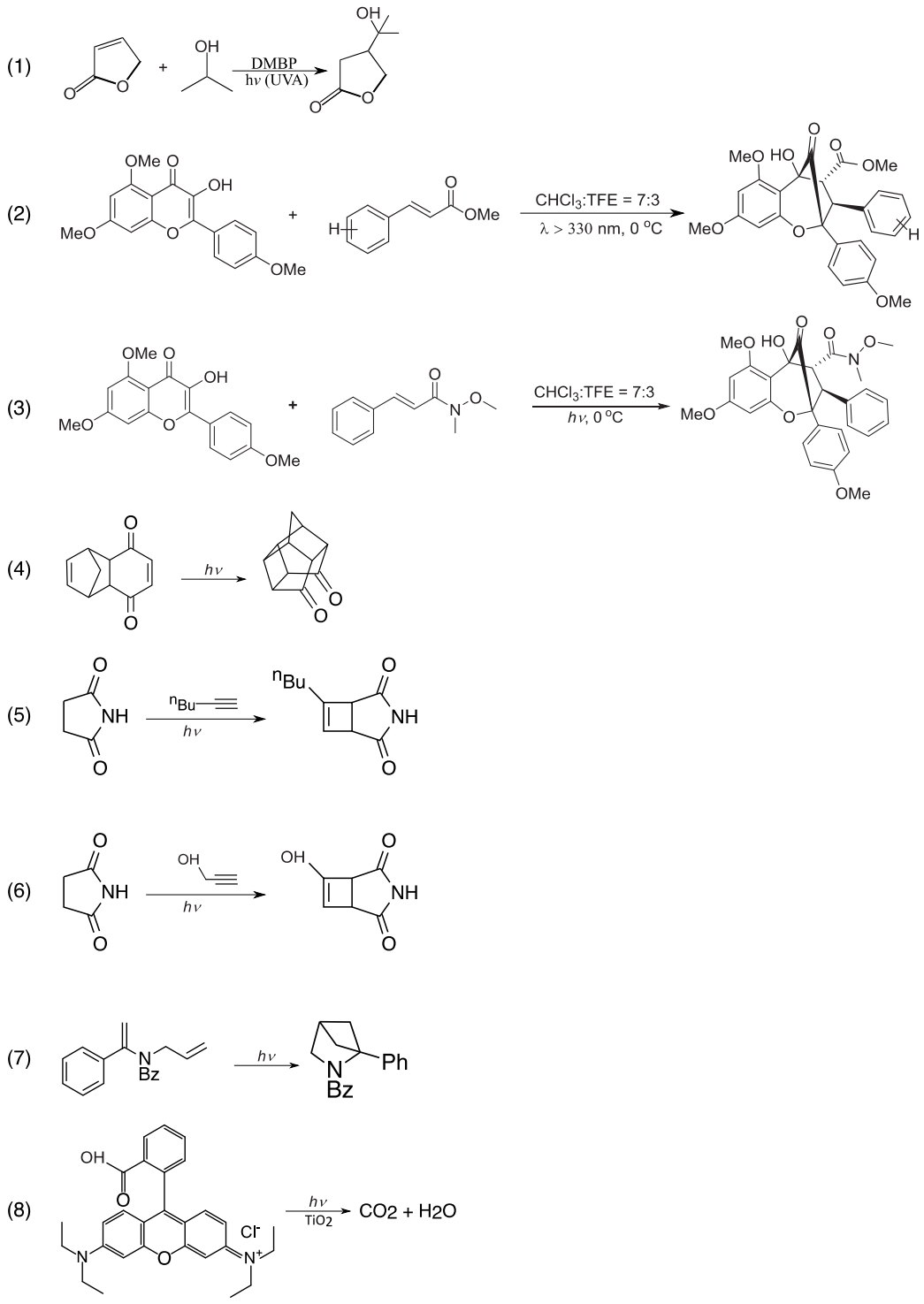

Figure 4. Photochemical reactions that are presented in Table 1.

Table 1. Comparison of different reactors in terms of PSTY. τ is the residence time and C is the concentration of the reactant. STY and PSTY are calculated based on Equation 4 and 5, respectively.

Entry	Reactor type	Volume (mL)	τ (min)	Reaction	Lamp power (W)	C (mM)	Yield	STY (mmol·L^{-1}·min^{-1})	PSTY (mol·day^{-1}·kW^{-1})	Ref
1	Microcapillary photoreactors (Figure 3a)	50.00	5.0	1	36.0	33.3	0.71	4.72	9.43	[31]
2			10.0				0.94	3.13	6.26	
3	Commercial microchip	0.02	2.5	1	0.5	33.3	0.89	11.87	0.57	[32]
4	Microcapillary photoreactors (Figure 3b)	37.50	35.0	2	450.0	120.0	0.61	2.09	0.25	[35]
5		37.50	35.0	3	450.0	120.0	0.35	1.20	0.14	
6		12.00	20.0	3	300.0	120.0	0.32	1.92	0.11	
7		3.50	30.0	3	150.0	120.0	0.36	1.44	0.05	
8	Fluoropolymer microcapillary films (Figure 3c)	0.15	0.5	removal of indigo carmine dye	8.0	0.2	0.70	0.30	0.01	[33]
9	Firefly reactor (Figure 3d)	120.00	76.0	4	3000.0	1000.0	0.88	11.58	0.67	[36]
10			151.0	4	1500.0	500.0	0.89	2.95	0.34	
11			227.0	4	3000.0	1000.0	0.89	3.92	0.23	
12			76.0	5 & 6	3000.0	100.0	0.65	0.86	0.05	
13			1342.0	7	3000.0	400.0	0.86	0.26	0.01	
14	Microchip (Figure 3e)	1.00	960.0	8	0.2	0.012	0.78	9.74E-06	7.01E-05	[34]
15		0.80	960.0				0.85	1.06E-05	6.12E-05	
16		0.50	960.0				0.86	1.08E-05	3.89E-05	
17		0.01	480.0				0.98	2.46E-05	1.77E-06	
18		0.02	240.0				0.97	4.88E-05	7.02E-06	
19		0.04	120.0				0.98	9.76E-05	2.81E-05	
20		0.06	60.0				0.98	1.96E-04	8.48E-05	

In a previous study, a microcapillary reactor (1/6” OD, 3.5 ml reactor volume) which was wrapped around a metal halide UV lamp was scaled up by using several strategies together. Rather than splitting up the reaction medium into many photoreactors, the photoreactors were numbered up by adding them in series (Figure 3b). That allowed a larger reactor volume with the same illumination. The throughput was increased by using a larger volumetric flow rate. Several [3+2] photocycloadditions were performed. While scaling up, the concentration of the reactants, the diameter of the tubes and the number of the reactors were increased systematically. The throughput was increased

around 20-folds by increasing the reactant concentration from 30 mM to 120 mM. The throughput was further increased by changing the diameter of the capillary from 1/6" to 1/8". Finally, three reactors were connected in series, which resulted in a reactor volume of 37.5 ml. By using three reactors in series with a larger capillary diameter, the throughput was increased from 0.14 g/L to 1.16 g/L. Similar yields were obtained in each step by adjusting the residence time [35]. Highest PSTY of this paper was calculated as 0.25 $mol \cdot day^{-1} \cdot kW^{-1\,-1}$ when 37.5 mL reactor was used (Table 1, entry 4). The PSTY value was decreased to 0.14 $mol \cdot day^{-1} \cdot kW^{-1}$ with a different reaction although the reaction conditions were the same (Table 1, entry 5). When smaller reactor volumes were used, PSTY was decreased further (Table 1, entries 5, 6 and 7). The PSTY was expected to stay approximately the same when the reactors were connected in series since the lamp power and the throughput were increased at the same level. However, in entries 5, 6 and 7, in addition to using more reactors in series, the microcapillary diameter was also changed which, in turn, changed the PSTY. The PSTY values of this paper were quite low considering that the authors followed a systematic way of scaling up by utilizing several strategies together. The low PSTY might be associated with the challenging synthesis reactions chosen in the paper. Previously, the synthesis of rocaglate was reported with even a higher lamp power (450 W) in a Pyrex test tube (16 x 100 mm) [37].

Fluoropolymer microcapillary films were suggested as another scale up approach (Figure 3c). These microcapillary films were produced commercially by Lamina Dielectrics Ltd (UK). The internal diameters of the microcapillaries range from 10 µm to 1 mm. The microcapillary films are transparent to UV and visible light. Furthermore, they have a refractive index close to water (~1.33), which makes them good candidates

for photochemical reactors. In one study, those microcapillary films were used for the photodegradation of indigo carmine, diclofenac and benzoylecgonine. The reactor volume was 0.15 ml [36]. The PSTY of the photodegradation of indigo carmine was calculated as 0.01 $mol \cdot day^{-1} \cdot kW^{-1}$ (Table 1, entry 8). In another study, those microcapillary films were used to synthesize ascaridole, an antimalarial drug, from α-terpinene by utilizing singlet oxygen. The permeability of the fluoropolymer film to oxygen was utilized to supply oxygen to microcapillaries. The system was suggested to be used in combination with dangerous gasses to ensure safe operational conditions. With the fluoropolymer microcapillaries, space time yields 20 times larger than the corresponding bulk synthesis were obtained [38]. Although it was suggested that fluoropolymer films could be easily scaled up by numbering up, how the flow was distributed to the microcapillaries was not explained in those studies [36], [38].

In another scale up study, quartz tubes were assembled in series and placed axially around a high-power UV lamp as shown in Figure 3d. The reactor had an internal volume of 120 mL. The photoreactor was enclosed with an annular metal cavity that reflect UV-radiation back to the reactor and served as a UV-protection. However, the metal cavity caused overheating. Therefore, a cooling jacket around the metal cavity was implemented in the design along with a fan to blow air through the space between the lamp and the quartz photoreactor tubes. The design was called Firefly reactor. Various [2+2] cycloadditions were performed in this reactor. Although similar amounts of starting material were used, the residence time varied significantly among different photoreactions to achieve the same yield [33]. The highest PSTY was calculated as 0.67 $mol \cdot day^{-1} \cdot kW^{-1}$ (Table 1, entry 9). This was the second highest PSTY among the photoreactors compared in this paper. However, the PSTY ranged between 0.23 and

0.67 mol·day^{-1}·kW^{-1} (Table 1, entry 9, 10 and 11) depending on the residence time, lamp power and the initial reactant concentration although the same reaction was used and similar yields were obtained. Therefore, a higher residence time reduced PSTY around three times since the yield did not improve further (Table 1, entries 9 and 11). When different reactions were used, the same reactor resulted in PSTY's of 0.01 and 0.05 mol·day^{-1}·kW^{-1} (Table 1, entries 9 and 11). This study demonstrated that optimization of process conditions and the kinetics of the selected reaction can lead to drastic changes in PSTY.

Sá et al [34] combined external and internal numbering-up in meso and microchemical reactors of various sizes (Figure 3e). The photocatalytic degradation of Methylene blue, Rhodamine B and phenol with TiO_2 were performed. Multiple microreactor units were connected to each other to increase the volume of the reactor while keeping the benefits of a microreactor. The reaction mixture was fully recycled when it left the reactor. Therefore, the reactor was operated as a batch reactor. Due to the small characteristic length of the reactor, there were less mass and photon transfer limitations compared to a conventional batch reactor [34]. Numbering-up was more beneficial in terms of STY and PSTY compared to increasing the dimensions as shown in Table 1 entry 14-20. Increasing the volume from 0.5 ml to 1 ml by increasing the dimensions decreased the STY by 10% whereas it increased the PSTY by 45%. When scaling up a reactor by increasing its dimensions, the surface to volume ratio decreases. This explains why the STY decreases, since the illuminated catalyst area per volume decreases which leads to an increase in mass transfer limitations and in turn, leads to lower apparent reaction rate and productivity. The PSTY increased since the same lamp was used to illuminate a larger reactor volume. Increasing the volume

of the reactor by numbering-up increased the STY and the PSTY by 97 and 98%, respectively. This is due to the increased total irradiated area while keeping the same surface to volume ratio.

Tree like structures (bifurcation configuration) have been used to distribute flow to many channels in various fields of research. Su et al. applied this numbering up approach to a capillary multiphase photoreactor by using the photocatalytic oxidation of thiols to disulfides as a model reaction. Two, four and eight photomicroreactors each having 0.5 mm internal diameter and 0.95 mL volume were connected in parallel by using T-junctions. The fluid is distributed in a tree like structure. A stable Taylor flow was obtained. The standard deviation of the flow distribution was less than 10%. The relative deviations of the liquid flow rate and the yield in each channel were found to be less than 4% [9]. Such a tree like structure was also utilized in the scale up of luminescent solar photomicroreactor which was fabricated via 3D printing [39]. Luminescent solar concentrators have been used in photovoltaic cell research for a couple of decades [40]. Noel's group combined the use of luminescent solar concentrators with microfluidics to harvest solar radiation into a narrow wavelength region and derive photochemical reactions [41]–[43]. By distributing the flow with a tree like structure, the luminescent solar photomicroreactor was operated with 32 channels with less than 10% standard deviation in flow distribution [39].

Enlarging one dimension while keeping rest of the dimensions constant is another scale up strategy. This strategy has been applied in commercial Corning Advanced-Flow reactors. Heart shapes provide good mixing for liquid and gas phase and enhance mass transfer while using the space on the microreactor chip efficiently. A photo of a

Corning reactor is given under mass transfer section (Figure 5c). Corning is offering reactors with different internal volumes. The lab scale reactor has an internal volume of 2.6 mL whereas the G1 and G3 photoreactors have internal volumes of 9 mL and 60 mL, respectively. All Corning reactors have the same heart shape static mixers [44]. Photocatalytic oxidation of methionine was performed in the Corning lab reactor. Two LED panels coupled with heat exchangers were placed on both sides of the reactor. Flow was supplied with an HPLC pump. Full conversions were achieved with residence times ranging from 0.6 min to 1.4 min. This reaction could be scaled up using other Corning reactors. For example, if the same conditions could be maintained in Corning G3 reactor, this reaction would have a productivity of 100 mol/day [45]. The power consumption of the LEDs was not reported in the paper. Therefore, the PSTY could not be calculated.

Packed bed structures are often used for mass transfer enhancement. Once the channel size is adjusted, translucent packed structures can be used as an alternative scale up strategy to numbering up of microreactors. Claes et al. adjusted the sizes of the beads in a catalytic packed bed reactor so that several microchannels were created among the beads. Glass beads were coated with TiO_2 photocatalyst. The photoreactor was illuminated with 192 LEDs that could provide 100 mW of power each. The distance between the LED board and the reactor was adjusted to give a uniform illumination which resulted in a high light efficiency [15].

A novel approach to scale up microreactors is to use an aerosol photoreactor. In this reactor concept, micron-sized droplets are generated using a nebulizer. Each droplet works as a microreactor. The high surface area of the droplets enables fast mass

transfer. As a result, aerosol photoreactor offers a great platform especially for gas-liquid or gas-liquid-solid photoreactions. When light hits a droplet, it is scattered. Therefore, the nature of the aerosol-light interactions enables good light distribution to all droplets. The reactor concept is easily scalable by simply increasing the number of nebulizers. An aerosol photoreactor called NebPhotOX has recently been operated several times and has been proved to work extremely efficiently [46]–[48]. In that work, the liquid reactants were nebulized into a glass chamber which was wrapped with LED strips. A pneumatic nebulizer was used. The droplet diameter was reported by the nebulizer supplier as 6 µm for water-based solutions. The droplet size depends on the surface tension and viscosity of the liquid and the pressure of the gas. Therefore, it might be different for different solvents that were used in the photoreactor. Several singlet oxygen mediated photooxidation reactions were performed in the aerosol photoreactor. Singlet oxygen is highly reactive state of oxygen which can be formed by some photosensitizers or dyes when an appropriate light source is used. The author performed ene reaction of β-citronellol and Diels-Alder reactions of α-terpinene and (5-methylfuran-2yl)methanol [46], synthesis of cyclopent-2-enones from furans [47] and synthesis of diverse γ-lactam scaffolds [48]. Conversions larger than 90% were achieved for all the reactions [46]–[48]. If the droplets are assumed to move with the gas, the residence time of the reactor would be around one minute. The PSTY of those papers could not be calculated as power consumption of LEDs were not reported. Aerosol photoreactors are quite promising as they can solve the bottleneck of the photoreactor design which is distribution of light efficiently in a large-scale reactor. Still, light efficiency of aerosol reactors requires further work as it would depend on the droplet diameter, the aerosol number concentration which is the total number of droplets per unit volume and the light path of the reactor. The major drawback of the

aerosol photoreactor is safety issue, especially for the organic oxidation reactions. Spraying organics into air or oxygen could be explosive. Therefore, the lower and upper explosion limits for the several organic photooxidation reactions should be determined in order to ensure safe operating conditions.

Mass transport

The mass transport phenomena can be quantified by the characteristic mixing time and the overall volumetric mass transfer coefficient. The characteristic mixing time in conventional reactors depends on many parameters such as diffusivity, kinematic viscosity, reactor volume, stirrer speed, etc. For laminar flow in microstructured reactors, the characteristic mixing time can be calculated by the Einstein-Smoluchovski equation (Equation 6). Due to the short diffusion distances, complete mixing can be achieved rapidly. That is the reason why microreactors are suitable for reactions with a high intrinsic reaction rate [11].

$$t_m = \frac{L^2}{D} \tag{6}$$

where t_m is the characteristic mixing time, L is the diffusion path and D is the molecular diffusivity.

The relative importance of characteristic mixing time in microreactors to the characteristic reaction time is given by the second Damköhler number (Da_{II}) (Equation 7). When Da_{II} is smaller than 1, the reaction is reaction-rate limited. In this region, further mixing does not affect the reaction rate. When Da_{II} is around 1, the reaction is controlled by both the reaction rate and mass transport. When Da_{II} is larger than 1, the

reaction is mass-transport limited. The residence time needs to be larger than the characteristic reaction time to achieve complete conversion [11].

$$Da_{II} = \frac{Reaction\ rate}{Diffusive\ mass\ transfer\ rate} = \frac{t_m}{t_r} \quad (7)$$

where t_r is the characteristic reaction time which can be loosely defined as the inverse of the reaction rate constant

Many photoreactions are heterogeneous, which means that the reaction requires the presence of at least two phases. Heterogeneous reactions require either a solid photocatalyst in a liquid medium or gas and liquid phases as the reactants. The mass transport and mixing gain extra importance in such systems. Mass transport is usually represented by the ratio of catalyst surface area to reaction volume in photocatalytic systems. The photocatalyst could be either mixed with reactants and fed into the reactor (slurry systems) or immobilized on a reactor surface. Slurry reactors remain the most preferred photoreactors due to the excellent contact between the catalyst and the reactants [2]. The ratio of the catalyst surface area to the reaction volume is quite high in slurry systems. However, the catalyst needs to be separated from the reaction medium in such systems, which adds complexity and additional costs to the overall process. It is possible to avoid the catalyst separation step with immobilized systems. Although they eliminate the catalyst separation step, the design of efficient immobilized systems is also quite challenging which requires complex mathematical models for the calculation of the internal mass and light transfer limitations. The catalyst thickness should be adjusted so that all the catalyst is utilized. The optimum catalyst thickness would depend on the interplay of many parameters such as the porosity of the catalyst and the support, flow rate of the reactants, the light distribution throughout the catalyst

layer and the reaction rate. Leblebici et al. [49] showed that increasing the flow rate of the reactants did not increase the apparent reaction rate for phenol degradation in an immobilized photoreactor. Increasing the flow rate would result in a higher driving force for the mass transfer when there are no internal mass transfer limitations. As a result, it was concluded that the internal mass transfer limitation of the catalyst coating limited the reaction rate. Therefore, increasing the catalyst layer does not necessarily increases the apparent reaction rate [49].

Structures are commonly used to alleviate the mass transport effects. Catalysts are usually coated on beads [15], [50], [51], monoliths [52]–[54] or foams [55]. Beads coated with catalyst are often used in packed bed photoreactors. A schematic representation of a packed bed photoreactor and a monolith is shown in Figure 5a and b. Performance of a capillary photomicroreactor packed with TiO_2 coated glass beads were compared with a photomicroreactor whose walls were coated with TiO_2. Degradation of methylene blue was chosen a model reaction. Complete conversion was achieved within 20 s when glass beads were used. The maximum space time yield of the packed bed photomicroreactor was found as 2322 $m^3.day^{-1}.m^{-3}$. On the other hand, in the wall coated photomicroreactor, the maximum space time yield was found as 356 $m^3.day^{-1}.m^{-3}$. The significant improvement in the space time yield was attributed to the larger ratio of the catalyst surface area to the reactor volume in the packed bed reactor as well as the flow perturbation that increases the mass transfer rate. In addition, the packed bed photomicroreactor showed good durability. The reactor performance dropped 17% after 6 h of operation and remained stable for the next 19.5 h [51]. Similarly, glass beads coated with photocatalysts were proved to increase the photoreaction rate twice in luminescent solar concentrator (LSC) photomicroreactor

with capillary channels [50]. Azam et al. studied monolithic honeycomb structures coated with La/TiO_2 for hydrogen production. The photocatalytic activity was increased 1.8 folds in the monolithic photoreactor as compared to the slurry photoreactor. The increased photocatalystic activity led to nine-folds higher hydrogen production rate in the monolithic photoreactor. The main reasons for this increase was the high surface area to volume ratio and better illumination of the monolithic photoreactor [56]. The monolithic photoreactor was shown to have higher yield for CO_2 photoreduction compared to a cell type reactor which had no channels. That was associated with better illumination efficiency and higher catalytic surface area [57].

There are several commercial photoreactors which are designed with static mixers to enhance mass transfer such as Hanu photoreactor and Corning Advanced-Flow™ reactors photoreactors (Figure 5c and d). The combination of an oscillatory flow with the static mixers of Hanu reactor (Figure 5c) enabled a stable suspension of photocatalysts without clogging of the reactor channels [58]. Corning flow reactors are designed to provide good mixing for multiphase reactions with periodic heart-shaped static mixers (Figure 5d). Two-phase flow transitions from Taylor flow to stratified flow and further to dispersed flow was investigated. The interfacial mass transfer and phase transitions were shown to be driven by fluid-structure interactions on the milli-scale. Therefore, this reactor design has a straightforward scalability with the same mass transfer characteristics by keeping the periodic heart-shaped static mixers [44].

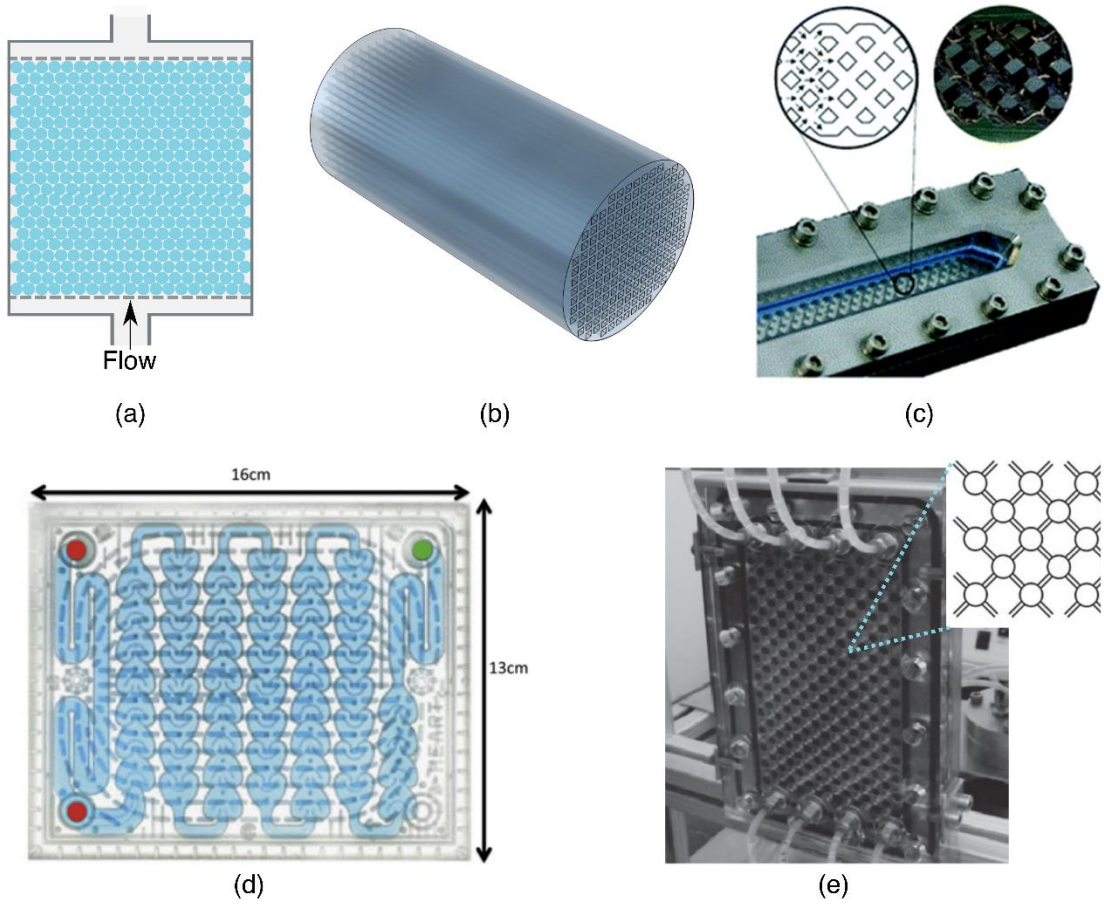

Figure 5. Structured reactors designed for enhancing mass transfer (a) Packed bed photoreactor (b) monolith reactor (c) Hanu reactor. Reprinted from *An oscillatory plug flow photoreactor facilitates semi-heterogeneous dual nickel/carbon nitride photocatalytic C-N couplings,* C. Rosso et al., React. Chem. Eng., vol. 5, pp. 597–604, 2020, [58], DOI: 10.1039/d0re00036a, licensed under a Creative Commons Attribution 3.0 Unported Licence, https://creativecommons.org/licenses/by/3.0/, (d) Commercial Corning Advanced-Flow™ reactors. Reprinted from *Scalability of mass transfer in liquid-liquid flow,* A. Woitalka, S. Kuhn, and K. F. Jensen, Chem. Eng. Sci., vol. 116, pp. 1–8, 2014 [44] DOI: 10.1016/j.ces.2014.04.036, licensed under a Creative Commons Attribution 3.0 Unported Licence, http://creativecommons.org/licenses/by/3.0/, (e) NETmix reactor. Reprinted from *The NETmix reactor: Pressure drop measurements and 3D CFD modelling*, C. M. Fonte, M. E. Leblebici, M. M. Dias, and J. C. B. Lopes, Chem. Eng. Res. Des., vol. 91, pp. 2250–2258, Copyright (2013) [59], with permission from Elsevier.

The NETmix reactor was originally developed by Brito Lopes et al [60]. The NETmix reactor was coated with TiO_2 photocatalyst for the removal of oxytetracycline (pharmaceutical micropollutant) from urban wastewater. The effect of a catalyst coated surface and the illumination mechanism was studied. When larger surface area was

coated with photocatalysts, the photocatalyst reactivity was increased [61]. Marinho et al. compared the performance of the NETmix reactor with a monolithic reactor packed with translucent cellulose acetate monolithic structures. The front glass of the slab, the network of the channels and the chambers imprinted in the back stainless-steel slab of the NETmix reactor were coated with a thin film photocatalyst (TiO_2-P25) by using a spray system. The catalyst reactivity in the NETmix reactor was 70-times higher than the monolithic photoreactor [62].

When the reactions involve a gas phase, Taylor flow, also known as slug flow, is commonly utilized in microstructured reactors. Su et al. studied the intrinsic kinetics of photocatalytic oxidation of thiophenol to phenyl disulfide using Taylor flow in a microreactor that consists of a capillary tube. By varying the flow rate of the gas and liquid phase and comparing the oxygen concentration in the liquid phase with its equilibrium concentration without reaction, the authors showed that mass transfer limitations were overcome in the microreactor [24].

Photon transport

A uniform light field is desired inside photoreactors. However, due to the exponential decay of light intensity along the light path, having a uniform light field throughout the reactor usually means that light is wasted. On the other hand, if utilization of all of the is light is desired, some of the reactor would be over-illuminated and the rest would be poorly illuminated. Reflective surfaces would eliminate this problem to some degree. Still, for an efficient photoreactor operation, the light source and its intensity need to be properly coupled with the reactor geometry. While selecting the light source, the light spectrum and energy efficiency of the lamp and shape of the reactor should be

considered. Ideally, the light source should emit light only at specific wavelengths that match the absorption spectrum of the photoactive molecule. In addition, the distance between the light source and the reactor should be taken into account while positioning the lamp. Irradiance pattern changes depending on the distance from the light source. At a far distance between the light source and the lamp, irradiance decreases with the square root of the distance from a point light source according to the inverse square law (Equation 8).

$$E \propto \frac{1}{d^2} \tag{8}$$

where *E* is the irradiance and *d* is the distance between the object and the light path.

At the near field, irradiance could be modelled with ray tracing algorithms or it could be measured experimentally with a near-field goniophotometer. The far-field for LEDs were usually assumed to start at a distance that is five times larger than the dimensions of the light source. In reality, the distance for the far field can go up to twenty times larger than the dimensions of the light source [63], [64]. As mentioned in the previous section, just adjusting the irradiance can lead to two orders of magnitude higher PSTY. Ziegenbalg et al. pointed out the importance of geometrical compatibility between the light source and the photomicroreactor by investigating a glass microreactor coupled with organic light emitting diodes. The authors showed that 63% of the photons were lost due to the mismatch between the reactor channels and the light source whereas 17% of the photons were lost due to the spectra mismatch [65]. While designing light sources, heat generated by the light sources should also be considered, as well. Excess heat can lead to damages of the whole set-up. In addition, the spectrum and the energy efficiency of the lamp can be affected by the temperature. For instance,

LED junction temperature affect the optical output power and spectrum of LEDs and, as a result, decrease the efficiency of the LEDs [66].

Light-emitting diodes (LEDs) are usually preferred to illuminate microstructured photoreactors due to their small size, monochromaticity and adjustable power. LEDs are also the most efficient light sources in the visible range [67]. Roibu et al. designed LED boards consisting of narrow viewing angle LEDs for an optimal coupling between the light source and the photomicroreactor. In Figure 6 a and b, the design of the two LED boards which were called the channel configuration (CC) and the matrix configuration (MC) were shown. The distance between the adjacent LEDs were 8 mm. The irradiance values at different distances (z) between the tip of the LED and the surface of the reactor was modelled with a ray tracing algorithm. The results were validated by experimental measurements. For these LED boards, optimum z-value where a uniform light distribution could be obtained on the surface of the photomicroreactor was found as 1.5 cm. The normalized irradiance values when z was 2 cm and 4 cm were shown in Figure 6 c,d,e and f. The most uniform irradiance was obtained with the CC array when z was 2 cm. The irradiance at the outer edges were lower compared to the central sections for MC array. The irradiance becomes more homogenous at the central sections when z was increased to 4. However, the overall uniformity decreased as the irradiance at the edges decreased even more. When the LEDs are configured in the same shape as the reactor, the energy efficiency was the highest [63].

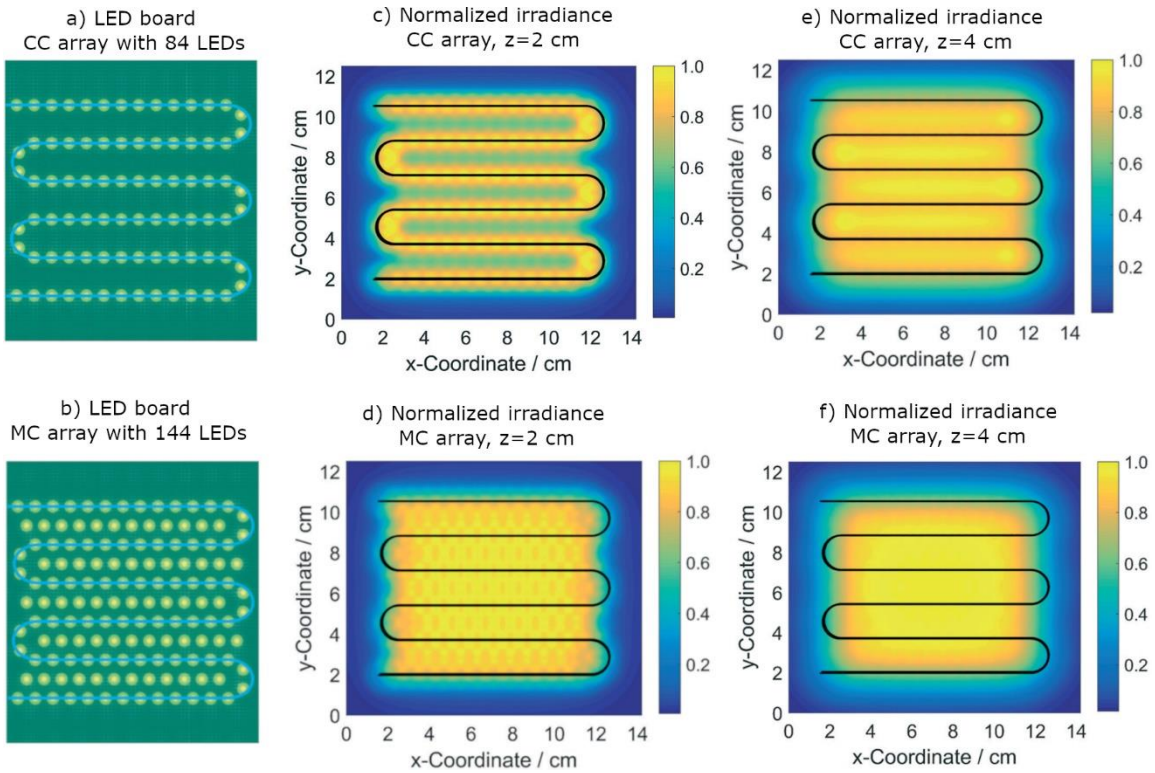

Figure 6. Comparison of design of LED boards for photomicroreactors. a) CC array design, b) MC array design. Normalized irradiance on a parallel plane placed, c) at z=2 cm from CC array, d) at z=2 cm from MC array, e) at z=4 cm from CC array, f) at z=4 cm from MC array. The photomicroreactor channels were represented with the S-shaped blue and black lines. The photomicroreactor dimensions are not drawn to scale. Reprinted from *Design and characterization of visible-light LED sources for microstructured photoreactors,* A. Roibu, R. B. Morthala, M. E. Leblebici, D. Koziej, T. Van Gerven, and S. Kuhn, *React. Chem. Eng.*, vol. 3, pp. 849–865, 2018 [63] with permission from The Royal Society of Chemistry.

As mentioned in the previous section, structures such as beads or monolith supports are frequently used to increase the mass transfer in photoreactors. Zhao et al. studied beads made of glass, zircon or steel in a capillary-based photomicroreactor. Opaque packing (steel) decreased the conversion by 5-15% depending on the flowrate. A material with a higher refractive index increased the conversion [50]. This is in line with the observations in the work of Cambié et al [43]. Ramos et al. also confirmed that utilization of transparent packed material increased the apparent reaction rate four-fold

compared to iron packing material [68]. Therefore, translucent material should be preferred in photoreactors.

Photon flux received by the absorbing species needs to be determined accurately in order to characterize photochemical reactors. Calculation of the local volumetric rate of photon (or energy) absorption (LVRPA or LVREA) is the main aspect of the modelling of photoreactors. LVRPA represent the amount of photons absorbed per unit time and per unit reactor volume at different locations in the reactor. Then, reaction rate at a given location can be related to the light field by using quantum yield (Equation 9). In order to obtain the average reaction rate, both the concentration field and the light field inside the reactor need to be solved. The concentration field inside the reactor depends on the hydrodynamics. For the ideal reactors (perfectly mixed or plug flow), the reaction rate would still be heterogenous due to the attenuation of the light inside the reactor [4]. The light field in single phase, homogenous photoreactions can be easily predicted by Beer-Lambert-Bouguer law (Equation 10).

$$-r = \phi\, LVRPA \tag{9}$$

where r is the reaction rate (mol·m^{-3}·s^{-1}), ϕ is the quantum yield (mol·mol photons^{-1}), *LVRPA* is local volumetric rate of photon absorption (mol·photon·m^{-3}·s^{-1}).

$$A = log_{10}\frac{E_0}{E} = \varepsilon l C \tag{10}$$

where A is absorbance, E_0 is the incident irradiance (W·m^{-2}), E is the irradiance transmitted by the medium (W·m^{-2}), $\boldsymbol{\varepsilon}$ is the absorptivity (m^2·mol^{-1}), l is the path length (m), C is the concentration of the attenuating species (mol·m^{-3}).

Photoreactions are often heterogeneous with solid particles in the reaction medium. In addition, some photoreactions contain a gas phase, which further complicates light

field models. In the case of heterogeneous photoreactions, liquid reaction medium is usually transparent to light. Solid photocatalysts, on the other hand, are absorbing and scattering light. Scattering of light by a particle depends on refractive index of the medium and the particle, the particle size and the wavelength of light. The ratio of the diameter of the particle to wavelength of light is called size parameter. Scattering phenomena in a tubular reactor is depicted in Figure 7.

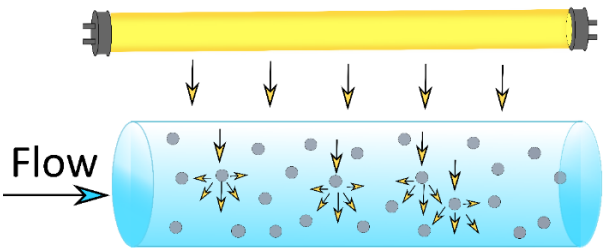

Figure 7. Illustration of light scattering phenomena inside a photocatalytic flow reactor

The efficiency of absorption in a scattering media with respect to purely absorption situations is shown in Figure 8. The optical thickness is the natural logarithm of the ratio of the incident to transmitted irradiance. The efficiency of the absorption process approaches to one at large optical thickness. At optically thick mediums, the mean free path of a photon gets so short that the medium could be considered like a continuum at constant optical thickness [69].

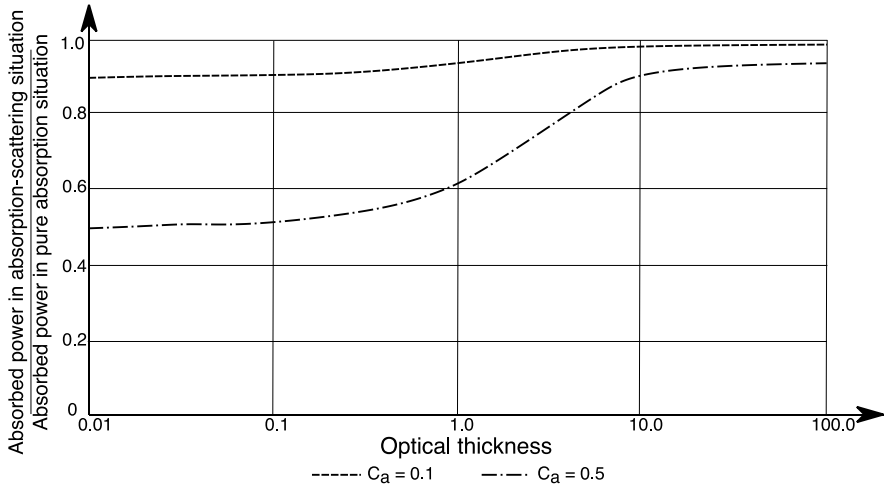

Figure 8: Efficiency of the absorption process in scattering situations with respect to purely absorption situations. The figure is redrawn from Spadoni et al [69].

The scattering by a single particle is described by Mie's theory. Gustav Mie solved the Maxwell equations for a plane electromagnetic wave encountering a sphere. Mie's theory gives exact analytical solutions for all size parameters. Still, Rayleigh scattering is preferred for small size parameters. For large size parameters, ray tracing which is also called geometric optics is less computationally demanding and therefore more frequently used in this region. Once the scattering profile of a photocatalyst particle is obtained, the radiative transfer equation still needs to be solved to obtain LVRPA. The integro-differential nature of the equation makes it quite hard to get an analytical solution. Therefore, approximations such zero reflectance [70], two flux [71] and six flux [72] were suggested to model the slurry photocatalytic systems. Among the simplified models, two flux gives a simple and still accurate solution of the radiative transfer equation in a scattering media. The model assumes the particles are purely backscattering the photon. The six flux model assumes that photons flow the six routes of the coordinate system. Therefore, it is more accurate. Six-flux is slightly more complex than two-flux approximation, but it is still an analytical equation that could be

easily calculated if the single scattering albedo is known. If absorbance of the photocatalyst is known, single scattering albedo could be obtained by using online tools which solves Mie's theory [73]. In the case of solid photocatalysts, the absorbance is usually unknown. Therefore, the single scattering albedos for solid photocatalysts are usually obtained experimentally.

Scattering phenomena are seen in all dimensions while designing a photoreactor. Not only the structures in the photoreactors but also the reactor tubes would scatter light when a bundle of tubes is illuminated. In a previous study, three different configurations of tube bundles in a 20 mm tube photoreactor were studied. The tube bundle consisted of 31 tubes of 3 mm outer diameter, 19 tubes of 4 mm outer diameter and 6 tubes of 8 mm outer diameter. An array of 6 tubes resulted in the best performance. The authors concluded that effectively illuminated surface area is of secondary importance in the design of tube bundles [74]. Jacobs et al. used ray tracing to model a 3D-printed translucent monolith. The diameter (D), number of channels and distance between the channels (L) were varied in the model. The optimal L/D ratio was found as two. Increasing the number of channels stacked upon each other up to 6 channels increased the amount of absorbed light and PSTY with the cost of increased inhomogeneous irradiation. Since translucent monoliths do not have the disadvantages of an optical fiber reactor, they showed an improvement of seven order in magnitude in terms of PSTY compared to internally illuminated monoliths.

Gas-liquid reactions in a photomicroreactor uses Taylor flow which is characterized by the regularly sized bubbles surrounded by liquid slugs. The light distribution is affected by the presence of bubbles in Taylor flow. In a recent study, a photochemical reaction

model was developed to optimize the performance of reactors which uses Taylor flow in a serpentine shaped photomicroreactor. The photon flux per liquid volume was shown to increase exponentially with the amount of gas inside the channels. Conversion was significantly affected by the liquid distribution inside the channels rather than the light scattering or the liquid mixing. In this work, an empirical formula was suggested for the prediction of optical path length in gas-liquid flows [75]. The photon transport together with hydrodynamics in the commercially available Corning® G1 Advanced Flow™ reactor (G1 AFR) was studied. A Corning AFR was shown in the previous section in Figure 5d. It was concluded that the photon flux per unit volume and the hydrodynamics did not depend on the gas content for a wide range of flow conditions, which showed the high flexibility of AFR. In this work, an empirical formula was suggested for the optical path length [76].

Utilization of solar energy for photoreactions can significantly reduce the cost of the process. In order to use to solar energy effectively, the use luminescent solar concentrators (LSC) together with flow photochemistry were offered. LSCs are devices in which luminophores such as fluorescent dyes or quantum dots are dispersed in a glass or polymeric material to capture the sunlight. The luminophore absorbs sunlight and can emit a specific wavelength of light. LCSs have often been coupled with photovoltaics. Cambie et al. embedded a microstructured photoreactor in a luminophore. The reactor was benchmarked with a [4+2] cycloaddition. Monte Carlo ray tracing simulations showed that the aspect ratio of the channels, the relative height of the channels compared to the device thickness and the number of channels per unit area were the most important design parameters [41]. In a recent work, the efficiency of the photomicroreactors embedded in LSC was demonstrated for many homogenous

and heterogenous photoreactions which span the entire visible spectrum. An autonomous control system which changed the residence time based on the fluctuations of solar light intensity was successfully operated [43]. These operations of photomicroreactors embedded in LSC are quite promising since they have the potential to reduce the energy costs significantly.

Flow distribution and fabrication of microreactors

Homogenous distribution of the fluids while numbering up microreactors is still one of the challenges while numbering up. A non-uniform flow distribution can cause a plethora of problems such under- and over-irradiation and a lower conversion. The maldistribution index (MI) is a common method to assess the flow distribution in internally scaled up reactors [9], [77]–[80]. It is defined as the relative standard deviation of the mass flowrate inside the microreactors or channels. This is shown in Equation 11.

$$MI = \sqrt{\frac{1}{n-1}\sum_{i=1}^{n}\left(\frac{q_i - \bar{\bar{q}}}{\bar{q}}\right)^2} \cdot 100\% \qquad 11$$

where n is the number of channels, q_i is the mass flow rate in a channel and $\bar{q}$ is the mean flow rate. A low MI indicates a uniform flow distribution.

Numerous distributors can be used to number-up photochemical microreactors. These are not limited to the field of photochemistry and inspiration can be found in the field of heat exchangers and other microreactors. These distributors are categorized and shown in Figure 9. When selecting a distributor to scale-up (photo)chemical microreactors by numbering up, a careful consideration based on the flow rate, amount

of channels and phases that needs to be distributed in the microreactors must be made.

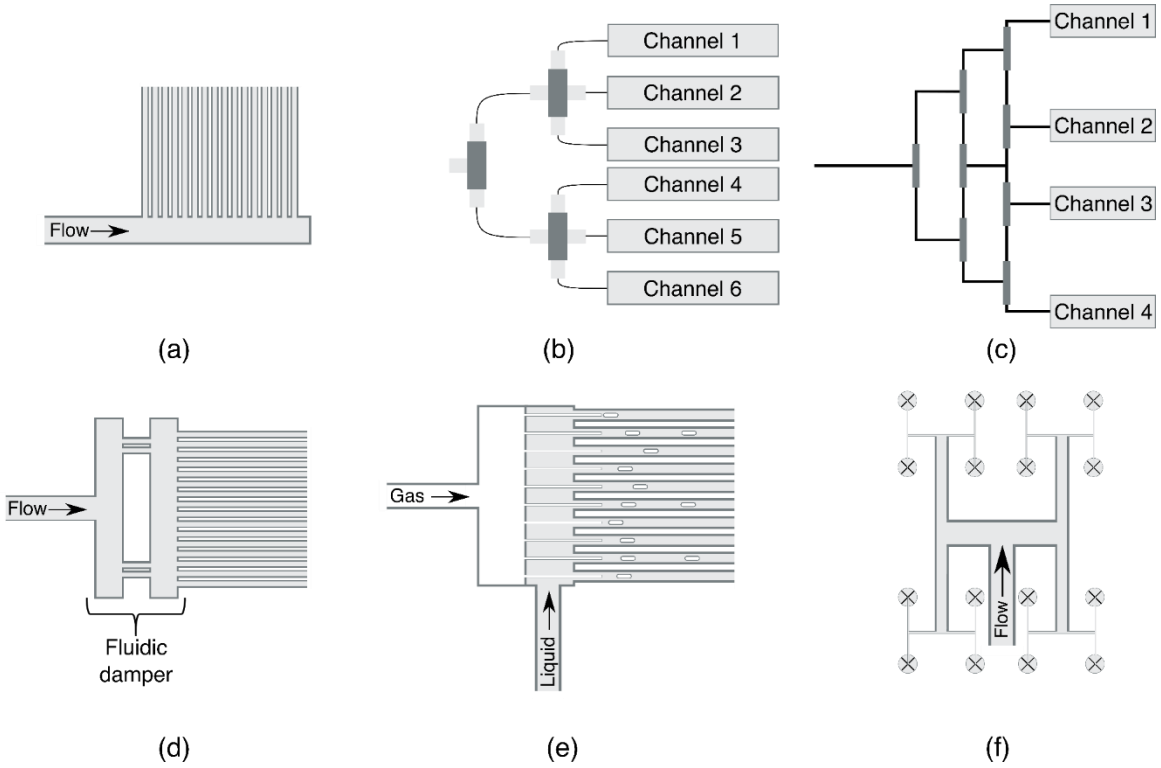

Figure 9. Different types of distributors (a) Traditional or consecutive manifold (b) Bifurcation unit distributing flow to 6 microreactors (MR) (c) Split-and-recombine (d) Distributor with fluidic damper (e) Needle distributor (f) Fractal distributor, channels are perpendicular to the plane of the paper and are depicted with an X.

The traditional manifolds, also known as consecutive manifolds, are one of the most used distributors for microreactor arrays due to their simplicity and their well-known design rules. They are used for single phase reactions at a low flow rate. Discrete methods are used to study the flow distribution and pressure drop in manifold systems. In these methods, a lattice network of resistances describes the system, which is analogous to electrical resistance networks. The flow rate is assumed to be linear related to the pressure drop. The Darcy-Weisbach equation or Hagen-Poiseuille equation is used in combination with Kirchhoff's law to predict the flow rate in each channel [81]–[84]. A consecutive manifold is shown in Figure 9a. It is also possible to

perform computational fluid dynamics (CFD) simulations to design a distributor. However, the resistance network models are usually preferred over CFD studies due to its simplicity [85].

A bifurcation manifold finds its inspiration in nature (e.g. trees, blood vessels and lungs). The flow is divided by tree-like structures as shown in Figure 9b. The same discrete methods of consecutive manifolds can be used to design a bifurcation distributor [83]. In contrast to the consecutive manifold, this distributor can be used to distribute gas and liquid efficiently [9]. Furthermore, the homogeneity of the flow distribution does not change for different flow rates if all the channels have the same characteristic length [83]. However, when a part of the network clogs, all downstream microreactors will suffer from this. Nagaki et al. have developed a split-and-recombine bifurcation distributor to mitigate the aforementioned issue by recombining the flow after each level of distribution as shown in Figure 9c [86].

When high flowrates are used in manifolds, the flow distribution will most likely not be uniform due to the inertial force [87]. It is known that placing baffles or a fluidic damper, with protrusions or holes, increases the hydraulic resistance so that a uniform flow can be obtained. Park et al. developed a method to design distributors containing baffles to obtain a uniform flow while utilizing a high flowrate [87]. Furthermore, this design can be used when the system contains a large number of microreactors, which is not the case with bifurcation manifolds. This design type is shown in Figure 9d.

A different approach to distribute fluid and gas over a stack of microreactors is to put needle-like structures inside the channels as shown in Figure 9e. This distributor was

able to distribute the flow over 357 channels with a MI lower than 3% [88], [89]. Fractals are self-similar repeating geometric structures which are invariant when scaling up or scaling down [90]. Mazur et al. obtained a MI of 1.63% when distributing fluid with a fractal distributor over 64 channels at a Reynolds number of 10 000. Thus, making the fractal distributor an interesting option when picking a suitable distributor for the microreactor [91]. A method to optimize this type of distributor is presented in the work of Wang et al. They used the lattice Boltzmann method to optimize the shape of a fractal distributor to obtain a lower pressure drop [92]. The lattice Boltzmann method is an alternative to traditional CFD methods to calculate the flow field. A pressure drop reduction between 15.9% and 25.1% was obtained by shape optimization in which the T-junctions evolved in Y-junctions by the algorithm. The design of fractal distributors is shown in Figure 9f. A comparison of the different distributors is shown in Table 2, this table can be used to select a suitable distributor.

Table 2. Comparison of different distributors.

Type	Phase	Inlet liquid flow rate (mL/min)	Reynolds number inlet (/)	Number of microreactors fed	MI (%)	Ref
Consecutive manifold	Liquid	0.01	0.1-10	10	0-16	[93]
Consecutive manifold	Gas/Liquid	0.08-1.92	0-5	4	4.5	[94]
Bifurcation	Liquid	0.2-12	5-500	2-8	7-30	[77]
Bifurcation	Gas/Liquid	0.6-5.6	5-200	8	1-10	[9]
Split-and-recombine	Liquid	3	200	5	1.8	[86]
Manifold with fluidic damper	Liquid	250	1485	625	1.2	[87]
Needle distributor	Gas/Liquid	Superficial velocity fluid 0.018 - 0.07ms^{-1}	20-250	32-357	0.5-3	[88]
Fractal distributor	Liquid	2880	1000-100 000	16-64	0.84-3.04	[91]

The fabrication of these distributors and microreactors is not always straightforward due to the many available fabrication techniques and material constraints. The photoreactor material needs to be transparent, which limits the materials. Furthermore, the small dimensions of the channels and shape also limits the fabrication methods.

Advanced fabrication methods such as 3D-printing, micro-milling, laser microchanneling, photolithography, etching, hot embossing and casting were covered in recent review papers [95]–[97]. The next section will give an overview of the materials that are commonly used for photomicroreactors together with the advantages and disadvantages.

A popular material for the construction of photomicroreactors is PDMS. The most common fabrication method to make PDMS photoreactors consisting of two parts. In the first part a mold is created by 3D-printing, soft lithography, milling or by manually constructing it with objects. The second part consists of casting the PDMS in the mold and cure it. An advantage of PDMS is that it can be bonded to glass, silicon and itself by treating the surface with oxygen plasma, which oxidizes the surface. This treatment allows the construction of complex geometries by stacking multiple pieces of PDMS. This material is used in the research of Cambie et al. to fabricate a photomicroreactor with 32 parallel channels and a bifurcated flow distributor. They performed the [4+2] cycloaddition of 9,10-Diphenylanthracene (DPA) with singlet oxygen in acetonitrile [39]. Another example of the fabrication of a photomicroreactor is the work of Lamberti et al. in which they produced a microfluidic chip to degrade methylene blue utilizing TiO_2 as a photocatalyst [98]. Despite the fact that PDMS is utilized to fabricate

photomicroreactor, there are some limitations to this material, which includes a limited resistivity against organic solvents and absorption of small hydrophobic molecules [20], [99]. This issue can be solved by coating the surface with a protective coating. Table 3 can be used to select a material that is compatible with common solvents used in photochemistry.

Table 3. Common solvents used in photochemistry and solvent resistance of PDMS, PMMA and glass.

+ Resistant **0** Swelling or cracking may occur after long-term exposure **–** Immediate damage may occur	**Solvent resistance**		
	PDMS	PMMA	Glass
Water	+	+	+
Acetonitrille	+	0	+
Ethanol	0	0	+
Tetrahydrofuran	-	-	+
Benzene	-	-	+
Toluene	-	-	+
Acetone	0	-	+

Another polymer that can be used to make photomicroreactors is PMMA. It is noteworthy that PMMA has similar properties and has a wider variety of fabrication methods. However, it is not often used for the construction of photochemical reactors. This is due to it lower surface quality, which causes scattering of the light, making them less transparent [100]. Nevertheless, in the work of Cambié et al., PMMA is used as a waveguide instead of PDMS since more light (40%) is directed to the reaction channel due to the higher refractive index, which is 1.49 and 1.42 for PMMA and PDMS respectively [43], [101], [102]. Recently, a 3D-printer was used to fabricate a microchannel from PMMA while incorporating a photoactive monomer, 4,7-distyrene-2,1,3-benzothiadiazole (BTZ), in the reactor structure [103].This demonstrated that is possible to directly manufacture a photomicroreactor with 3D-printing, allowing a high

degree of design freedom. The direct manufacture of a photomicroreactor is also shown in the research of Guba et al [104].

Glass is an excellent material due its high optical transparence. The wavelength cutoff for quartz and borosilicate is 170 nm and 275 nm respectively. Furthermore, glass is more resistant to high temperatures and is inert to the majority of solvents used in photochemistry, as shown in Table 3 [105]. Due to the more complex fabrication techniques for glass, it is more expensive and time-consuming to make a glass photomicroreactor. The most common fabrication methods are micromilling, photolithography and wet etching. Takei at al. used a photomicroreactor with 16 channels created by photolithography and wet etching. The reaction zone was coated with TiO_2 to catalyze the synthesis of L-pipecolinic acid [16]. Usami et al. utilized a more exotic method to fabricate photoreactors consists in partially melting (sintering) glass beads to produce a highly interconnected transparent structure inside a cylinder. The photocatalytic degradation of 4-chlorophenol was performed in this reactor. Due to the high surface to volume ratio of the structure (6500 m^{-1}), there is a relative increase of 66 % in conversion compared to the reactor without this structure [106].

New techniques emerged to 3D-print complex glass microstructures that are required to scale up repetitive structures. Kotz et al. presented a 3D-printing method to fabricate microchannels with a characteristic length of 20 µm. Moreover, they showed the ability to 3D-print microchannels with a spherical, triangular, trapezoidal, and rectangular cross-section [107]. This allows the fabrication of complex geometries from glass necessary for the intensification of photochemical reactions.

Conclusion and Outlook

When combined with continuous flow mode, micro- and meso-structured photoreactors have the potential to enable efficient and safe operational conditions. As a result, there is a growing interest in micro- and meso-structured photoreactors leading to a “renaissance” of photochemistry. In this paper, we have discussed the flow and light distribution and mass transport issues in these photoreactors. It was concluded that not only the reactor geometry but also the operational conditions such as the concentrations of the photoactive molecules and the reactants, the residence time and the light intensity needed to be tuned for an efficient photoreactor operation. A proper coupling of the light source and reactor geometry is one of the major hurdles of high through-put photochemistry. It would be good to keep testing new reactor geometries in large scales where photon flux, mass transfer characteristics and flow dynamics are characterized. The technical challenges for different structured reactors differ widely. For example, aerosol photoreactors provide a great platform for multiphase reactions. However, if they are going to be used for photooxidations, the lower and upper explosion limits of aerosol should be studied further. For the photomicroreactors, technical challenges lie in the distribution of light and flow to all units of microreactors. Much work has been done on the design of flow distributors in two dimensions. However, more research needs to be done on the flow distribution in three dimensions. Different fabrication methods have different challenges. For example, 3D-printing is currently limited to certain polymers and metals which are usually not chemical inert, not UV-transparent or cannot handle high temperatures and pressures. Utilizing 3D-printing of glass in photochemistry would make a great contribution to this field.

Funding

Mumin Enis Leblebici thankfully acknowledges FWO-Flanders for a postdoctoral fellowship (39715).

References

[1] K.-H. Pfoertner and T. Oppenlander, *Ullmann's Encyclopedia of Industrial Chemistry*. Wiley-VCH Verlag GmbH & Co. KGaA, 2000.

[2] T. Van Gerven, G. Mul, J. Moulijn, and A. Stankiewicz, *Chem. Eng. Process. Process Intensif.*, vol. 46, pp. 781–789, 2007.

[3] J. Turconi *et al.*, *Org. Process Res. Dev.*, vol. 18, pp. 417–422, 2014.

[4] K. Loubière, M. Oelgemöller, T. Aillet, O. Dechy-Cabaret, and L. Prat, *Chem. Eng. Process. Process Intensif.*, vol. 104, pp. 120–132, Jun. 2016.

[5] D. J. Boston, C. Xu, D. W. Armstrong, and F. M. Macdonnell, *J. Am. Chem. Soc.*, vol. 135, pp. 16252–16255, 2013.

[6] A. Banerjee *et al.*, *J. Am. Chem. Soc.*, vol. 137, pp. 2030–2034, 2015.

[7] S. Bhatta, D. Nagassou, and J. P. Trelles, *Sol. Energy*, vol. 142, pp. 253–266, 2017.

[8] A. K. Suresh, *Ind. Eng. Chem. Res*, pp. 3958–3997, 2000.

[9] Y. Su, K. Kuijpers, V. Hessel, and T. Noël, *React. Chem. Eng.*, vol. 1, pp. 73–81, 2016.

[10] C. Sambiagio and T. Noël, *Trends Chem.*, vol. 2, pp. 92–106, 2020.

[11] Y. Su, N. J. W. Straathof, V. Hessel, and T. No, *Chem. Eur. J*, pp. 10562–10589, 2014.

[12] J. Herrmann, *Catal. Today*, vol. 53, pp. 115–129, 1999.

[13] A. Kumar, P. R. Gogate, and A. B. Pandit, *Ultrason. Sonochem.*, vol. 14, pp. 538–544, 2007.

[14] Y. A. Shaban, M. A. El Sayed, A. A. El Maradny, R. Kh, A. Farawati, and M. I. Al Zobidi, *Chemosphere*, vol. 91, pp. 307–313, 2013.

[15] T. Claes, A. Dilissen, M. E. Leblebici, and T. Van Gerven, *Chem. Eng. J.*, vol. 361, pp. 725–735, 2019.

[16] G. Takei, T. Kitamori, and H. Kim, *Catal. Commun.*, vol. 6, pp. 357–360, 2005.

[17] X. Li *et al.*, *ChemComm*, pp. 964–965, 2003.

[18] S. E. Braslavsky *et al.*, *Pure Appl. Chem.*, vol. 83, pp. 931–1014, 2011.

[19] G. J. Janz and S. C. Wait, *J. Chem. Phys.*, vol. 23, pp. 1550–1551, 1955.

[20] D. Cambié, C. Bottecchia, N. J. W. Straathof, V. Hessel, and T. Noël, *Chem. Rev.*, vol. 116, pp. 10276–10341, 2016.

[21] A. Roibu, 2019.

[22] M. E. Leblebici, G. D. Stefanidis, and T. Van Gerven, *Chem. Eng. Process. Process Intensif.*, vol. 97, pp. 106–111, 2015.

[23] T. Aillet, K. Loubière, O. Dechy-Cabaret, and L. Prat, *Chem. Eng. Technol.*, vol. 39, pp. 115–122, 2016.

[24] Y. Su, V. Hessel, and T. Noël, *AIChE J.*, vol. 61, pp. 2215–2227, 2015.

[25] A. Visan, D. Rafieian, W. Ogieglo, and R. G. H. Lammertink, *Appl. Catal. B Environ.*, vol. 150–151, pp. 93–100, 2014.

[26] M. L. Satuf, J. Macagno, A. Manassero, G. Bernal, P. A. Kler, and C. L. A. Berli, *Appl. Catal. B Environ.*, vol. 241, pp. 8–17, 2019.

[27] G. Li Puma and P. L. Yue, *Ind. Eng. Chem. Res.*, vol. 40, pp. 5162–5169, 2001.

[28] T. H. Lim and S. D. Kim, *Chemosphere*, vol. 54, pp. 305–312, 2004.

[29] H. C. Yatmaz, C. Wallis, and C. R. Howarth, *Chemosphere*, vol. 42, pp. 397–403, 2001.

[30] N. A. Hamill, L. R. Weatherley, and C. Hardacre, *Appl. Catal. B Environ.*, vol. 30, pp. 49–60, 2001.

[31] A. Yavorskyy, O. Shvydkiv, N. Hoffmann, K. Nolan, and M. Oelgemöller, *Org. Lett.*, vol. 14, pp. 4342–4345, 2012.

[32] O. Shvydkiv *et al.*, *Photochem. Photobiol. Sci.*, vol. 9, pp. 1601–1603, 2010.

[33] L. D. Elliott, M. Berry, B. Harji, D. Klauber, J. Leonard, and K. I. Booker-Milburn, *Org. Process Res. Dev.*, vol. 20, pp. 1806–1811, 2016.

[34] D. S. de Sá *et al.*, *J. Photochem. Photobiol. A Chem.*, vol. 364, pp. 59–75, 2018.

[35] H. Yueh, Q. Gao, J. A. Porco, and A. B. Beeler, *Bioorganic Med. Chem.*, vol. 25, pp. 6197–6202, 2017.

[36] N. M. Reis and G. Li Puma, *Chem. Commun.*, vol. 51, pp. 8414–8417, 2015.

[37] B. Gerard, S. Sangji, D. J. O'Leary, and J. A. Porco, *J. Am. Chem. Soc.*, vol. 128, pp. 7754–7755, 2006.

[38] K. S. Elvira, R. C. R. Wootton, N. M. Reis, M. R. Mackley, and A. J. DeMello, *ACS Sustain. Chem. Eng.*, vol. 1, pp. 209–213, 2013.

[39] F. Zhao *et al.*, *ACS Sustain. Chem. Eng.*, vol. 6, pp. 422–429, 2018.

[40] M. G. Debije and P. P. C. Verbunt, *Adv. Energy Mater.*, vol. 2, pp. 12–35, 2012.

[41] D. Cambié, F. Zhao, V. Hessel, M. G. Debije, and T. Noël, *Angew. Chemie - Int. Ed.*, vol. 56, pp. 1050–1054, 2017.

[42] D. Cambié, F. Zhao, V. Hessel, M. G. Debije, and T. Noël, *React. Chem. Eng.*, vol. 2, pp. 561–566, 2017.

[43] D. Cambié *et al.*, *Angew. Chemie - Int. Ed.*, vol. 58, pp. 14374–14378, 2019.

[44] A. Woitalka, S. Kuhn, and K. F. Jensen, *Chem. Eng. Sci.*, vol. 116, pp. 1–8, 2014.

[45] N. Emmanuel *et al.*, *Org. Process Res. Dev.*, vol. 21, pp. 1435–1438, 2017.

[46] G. I. Ioannou, T. Montagnon, D. Kalaitzakis, S. A. Pergantis, and G. Vassilikogiannakis, *ChemPhotoChem*, vol. 1, pp. 173–177, 2017.

[47] G. I. Ioannou, T. Montagnon, D. Kalaitzakis, S. A. Pergantis, and G. Vassilikogiannakis, *Org. Biomol. Chem.*, vol. 15, pp. 10151–10155, 2017.

[48] G. I. Ioannou, T. Montagnon, D. Kalaitzakis, S. A. Pergantis, and G. Vassilikogiannakis, *ChemPhotoChem*, vol. 2, pp. 860–864, 2018.

[49] M. E. Leblebici, J. Rongé, J. A. Martens, G. D. Stefanidis, and T. Van Gerven, *Chem. Eng. J.*, vol. 264, pp. 962–970, 2015.

[50] F. Zhao, Z. Chen, W. Fan, J. Dou, L. Li, and X. Guo, *Chem. Eng. J.*, vol. 389, p. 124409, 2020.

[51] S. Zhang, J. Zhang, J. Sun, and Z. Tang, *Chem. Eng. Process. Process Intensif.*, vol. 147, p. 107746, 2020.

[52] K. Te Lu *et al.*, *Chem. Eng. J.*, vol. 296, pp. 11–18, 2016.

[53] O. Ola, M. Maroto-Valer, D. Liu, S. MacKintosh, C. W. Lee, and J. C. S. Wu, *Appl. Catal. B Environ.*, vol. 126, pp. 172–179, 2012.

[54] B. A. Marinho, R. O. Cristóvão, R. Djellabi, J. M. Loureiro, R. A. R. Boaventura, and V. J. P. Vilar, *Appl. Catal. B Environ.*, vol. 203, pp. 18–30, 2017.

[55] S. Hajiesmaili, S. Josset, D. Bégin, C. Pham-Huu, N. Keller, and V. Keller, *Appl. Catal. A Gen.*, vol. 382, pp. 122–130, 2010.

[56] M. U. Azam, M. Tahir, M. Umer, M. M. Jaffar, and M. G. M. Nawawi, *Appl. Surf. Sci.*, vol. 484, pp. 1089–1101, 2019.

[57] M. Tahir and N. A. S. Amin, *Chem. Eng. J.*, vol. 230, pp. 314–327, 2013.

[58] C. Rosso *et al.*, *React. Chem. Eng.*, vol. 5, pp. 597–604, 2020.

[59] C. M. Fonte, M. E. Leblebici, M. M. Dias, and J. C. B. Lopes, *Chem. Eng. Res. Des.*, vol. 91, pp. 2250–2258, 2013.

[60] J. C. Brito Lopes, P. E. M. dos S. da C. Laranjeira, M. M. G. Q. Dias, and A. A. A. Martins, US 8,434,933 B2, 2013.

[61] J. C. Espíndola *et al.*, *Sci. Total Environ.*, vol. 681, pp. 467–474, 2019.

[62] B. A. Marinho *et al.*, *J. Environ. Manage.*, vol. 217, pp. 555–564, 2018.

[63] A. Roibu, R. B. Morthala, M. E. Leblebici, D. Koziej, T. Van Gerven, and S. Kuhn, *React. Chem. Eng.*, vol. 3, pp. 849–865, 2018.

[64] I. Moreno and C.-C. Sun, *Opt. Express*, vol. 16, pp. 1808–1819, 2008.

[65] D. Ziegenbalg, B. Wriedt, G. Kreisel, and D. Kralisch, *Chem. Eng. Technol.*, vol. 39, pp. 123–134, 2016.

[66] M. Bürmen, F. Pernu, and B. Likar, *Meas. Sci. Technol.*, vol. 19, p. 122002, 2008.

[67] M. Sender and D. Ziegenbalg, *Chemie-Ingenieur-Technik*, vol. 89, pp. 1159–1173, 2017.

[68] B. Ramos, A. P. Couri, S. Ookawara, and A. C. S. C. Teixeira, *ChemRxiv Prepr.*, vol. 6726395, pp. 1–9, 2018.

[69] G. Spadoni, E. Bandini, and F. Santarelli, *Chem. Eng. Sci.*, vol. 33, pp. 517–524, 1978.

[70] A. Brucato and L. Rizzuti, *Ind. Eng. Chem. Res.*, vol. 36, pp. 4740–4747, 1997.

[71] A. Brucato and L. Rizzuti, *Ind. Eng. Chem. Res.*, vol. 36, pp. 4748–4755, 1997.

[72] A. Brucato, A. E. Cassano, F. Grisafi, G. Montante, L. Rizzuti, and G. Vella, *AICHE J.*, vol. 52, pp. 3882–3890, 2006.

[73] M. P. (http://www. philiplaven. com/mieplot. htm#Downloa. MiePlot), .

[74] F. Denny, P. McCaffrey, J. Scott, G. D. Peng, and R. Amal, *Chem. Eng. Sci.*, vol. 66, pp. 3641–3647, 2011.

[75] A. Roibu, T. Van Gerven, and S. Kuhn, *ChemPhotoChem*, vol. 4, p. (in press), 2020.

[76] A. Roibu, C. R. Horn, T. Van Gerven, and S. Kuhn, *ChemPhotoChem*, vol. 4, p. (in press), 2020.

[77] M. Qiu, L. Zha, Y. Song, L. Xiang, and Y. Su, *React. Chem. Eng.*, vol. 4, pp. 351–361, 2019.

[78] M. Schultes, *Ind. Eng. Chem. Res.*, vol. 39, pp. 1381–1389, 2000.

[79] S. J. Yim, B. T. Ramanjaneyulu, S. Vidyacharan, Y. D. Yang, I. S. Kang, and D. P. Kim, *Lab Chip*, vol. 20, pp. 973–978, 2020.

[80] G. N. Ahn *et al.*, *Lab Chip*, vol. 19, pp. 3535–3542, 2019.

[81] J. Wang, *Chem. Eng. J.*, vol. 168, pp. 1331–1345, 2011.

[82] J. Wang and H. Wang, *Appl. Therm. Eng.*, vol. 89, pp. 927–945, 2015.

[83] C. Amador, A. Gavriilidis, and P. Angeli, *Chem. Eng. J.*, vol. 101, pp. 379–390, 2004.

[84] D. Tondeur, Y. Fan, J. M. Commenge, and L. Luo, *Chem. Eng. Sci.*, vol. 66, pp. 2568–2586, 2011.

[85] E. Garciadiego Ortega, D. Tsaoulidis, and P. Angeli, *Chem. Eng. J.*, vol. 351, pp. 589–602, 2018.

[86] A. Nagaki *et al.*, *Org. Process Res. Dev.*, vol. 20, pp. 687–691, 2016.

[87] Y. J. Park, T. Yu, S. J. Yim, D. You, and D. P. Kim, *Lab Chip*, vol. 18, pp. 1250–1258, 2018.

[88] T. Scha, S. Haase, and M. Lange, pp. 2058–2066, 2017.

[89] S. Haase and T. Bauer, *Chem. Eng. J.*, vol. 176–177, pp. 65–74, 2011.

[90] B. B. Mandelbrot and J. A. Wheeler, *American Journal of Physics*, vol. 51. pp. 286–287, 1983.

[91] M. Mazur *et al.*, *Chem. Eng. Process. - Process Intensif.*, vol. 143, p. 107595, 2019.

[92] L. Wang, Y. Fan, and L. Luo, *Comput. FLUIDS*, vol. 94, pp. 49–57, 2014.

[93] C. Renault, S. Colin, S. Orieux, P. Cognet, and T. Tzédakis, *Microsyst. Technol.*, vol. 18, pp. 209–223, 2012.

[94] M. Al-Rawashdeh, L. J. M. Fluitsma, T. A. Nijhuis, E. V. Rebrov, V. Hessel, and J. C. Schouten, *Chem. Eng. J.*, vol. 181–182, pp. 549–556, 2012.

[95] S. Das and V. C. Srivastava, *Photochem. Photobiol. Sci.*, vol. 15, pp. 714–730, 2016.

[96] B. K. Gale *et al.*, *Inventions*, vol. 3, 2018.

[97] N. Convery and N. Gadegaard, *Micro Nano Eng.*, vol. 2, pp. 76–91, 2019.

[98] H. Song and R. F. Ismagilov, *J. Am. Chem. Soc.*, vol. 125, pp. 14613–14619, 2003.

[99] Y. Wang, S. Chen, H. Sun, L. Wanbo, C. Hu, and K. Ren, *Microphysiological Syst.*, vol. 2, p. 6, Sep. 2018.

[100] C. Matellan, E. Armando, and R. Hernández, pp. 1–13, 2018.

[101] N. Sultanova, S. Kasarova, and I. Nikolov, *Acta Phys. Pol. A*, vol. 116, pp. 585–587, 2009.

[102] B. van Lierop *et al.*, *Spectra Identif. Addit. Food Packag.*, pp. 396–400, 1998.

[103] A. Zhakeyev *et al.*, *Energy Procedia*, vol. 158, pp. 5608–5614, 2019.

[104] F. Guba, Ü. Tastan, K. Gugeler, M. Buntrock, T. Rommel, and D. Ziegenbalg, *Chemie-Ingenieur-Technik*, vol. 91, pp. 17–29, 2019.

[105] J. P. Mcmullen and K. F. Jensen, 2010.

[106] H. Usami, K. Ohta, and S. Inagawa, *J. Photochem. Photobiol. A Chem.*, vol. 332, pp. 595–601, 2017.

[107] F. Kotz, P. Risch, D. Helmer, and B. E. Rapp, *Adv. Mater.*, vol. 31, 2019.